Exaggerated Eye Growth in IRBP-Deficient Mice in Early Development

Jeffrey Wisard,[1] Amanda Faulkner,[2] Micah A. Chrenek,[1] Timothy Waxweiler,[1] Weston Waxweiler,[1] Christy Donmoyer,[3] Gregory I. Liou,[4] Cheryl M. Craft,[5,6] Gregor F. Schmid,[2] Jeffrey H. Boatright,[1] Machelle T. Pardue,[2,1] John M. Nickerson[1]

Purpose. Because interphotoreceptor retinoid-binding protein (IRBP) is expressed before being needed in its presumptive role in the visual cycle, we tested whether it controls eye growth during development.

Methods. The eyes of congenic IRBP knockout (KO) and C57BL/6J wild-type (WT) mice ranging in age from postnatal day (P)2 to P440 were compared by histology, laser micrometry, cycloplegic photorefractions, and partial coherence interferometry.

Results. The size and weight of IRBP KO mouse eyes were greater than those of the WT mouse, even before eye-opening. Excessive ocular enlargement started between P7 and P10, with KO retinal arc lengths becoming greater compared with WT from P10 through P30 (18%; $P < 0.01$). The outer nuclear layer (ONL) of KO retinas became 20% thinner between P12 to P25, and progressed to 38% thinner at P30. At P30, there were 30% fewer cones per vertical section in KO than in WT retinas. Bromodeoxyuridine (BrdU) labeling indicated the same number of retinal cells were born in KO and WT mice. A spike in apoptosis was observed in KO outer nuclear layer at P25. These changes in size were accompanied by a large decrease in hyperopic refractive error, which reached -4.56 ± 0.70 diopters (D) versus $+9.98 \pm 0.993$ D (mean $\pm$ SD) in WT, by postnatal day 60 (P60).

Conclusions. In addition to its role in the visual cycle, IRBP is needed for normal eye development. How IRBP mediates ocular development is unknown. (*Invest Ophthalmol Vis Sci.* 2011;52:5804–5811) DOI:10.1167/iovs.10-7129

From the [1]Department of Ophthalmology, Emory University, Atlanta, Georgia; [2]Atlanta VA Medical Center, Rehabilitation Research Center of Excellence, Decatur, Georgia; [3]Biological Sciences, Allegheny College; [4]Medical College of Georgia, Augusta, Georgia; [5]Department of Ophthalmology, Keck School of Medicine of the University of Southern California; and [6]Doheny Eye Institute, Los Angeles, California.

Supported by Research to Prevent Blindness; the Foundation Fighting Blindness; Fight for Sight; NEI Grants R01EY016470, R01EY014026 (JHB); R24EY017405, P30EY006360, R01EY016435 (MTP); DM102155 (GIL); R01EY015851 (CMC); P30EY003040 (DEI core); Mary D. Allen Chair in Vision Research, Doheny Eye Institute (CMC), and the Rehabilitation Research and Development Service, Department of Veterans Affairs.

Submitted for publication December 22, 2010; revised April 18 and May 13, 2011; accepted May 16, 2011.

Disclosure: **J. Wisard**, None; **A. Faulkner**, None; **M.A. Chrenek**, None; **T. Waxweiler**, None; **W. Waxweiler**, None; **C. Donmoyer**, None; **G.I. Liou**, None; **C.M. Craft**, None; **G.F. Schmid**, None; **J.H. Boatright**, None; **M.T. Pardue**, None; **J.M. Nickerson**, None

Corresponding author: John M. Nickerson, Department of Ophthalmology, Emory University, B5602, 1365B Clifton Road NE, Atlanta, GA 30322; litjn@emory.edu.

Interphotoreceptor retinoid-binding protein (IRBP) is a 135 kDa glycoprotein found primarily in the subretinal or interphotoreceptor space (IPS) within the eye. IRBP binds retinoids and fatty acids,[1–6] accounts for 70% of the soluble protein in this space, and is the most abundant retinoid-binding protein in the IPS.[7] In mammals, IRBP is synthesized by photoreceptor cells and pinealocytes.[8,9] Mutations in IRBP can cause retinitis pigmentosa.[10]

Although the ligand-binding properties of IRBP are well known,[11–13] the biological functions of IRBP are not understood. IRBP isolated in the dark mainly binds 11-cis-retinal, while all-trans-retinol is recovered from IRBP of light-adapted eyes.[14] IRBP extracts 11-*cis*-retinal from RPE cells and membranes.[15–20] IRBP removes all-trans retinol from rod outer segments during bleaching.[18] These observations suggest that IRBP functions as a retinoid buffer,[21] consistent with measurements of vitamin A cycling and dark adaptation.[22]

Studies with an IRBP gene knockout (KO) mouse suggest a role for IRBP in the rapid regeneration of cone pigments. Under photopic ERG conditions with 10 Hz flickering light (a condition used to isolate cone responses), the IRBP KO mouse does not regenerate cone pigments as quickly as C57BL/6J (wild-type controls; WT).[23] However, in the dark, retinoids traverse the IPS faster in IRBP-deficient mice, such that functional rhodopsin is more rapidly regenerated after a strong light bleach.[24] Thus, it appears that cone pigment regeneration requires IRBP, and rhodopsin regeneration[23,25,26] does not.

In the KO mouse, the a-wave in scotopic electroretinograms (ERGs) is reduced by approximately 40%, and the thickness of the outer nuclear layer (ONL) is decreased proportionately by approximately 40% at postnatal day (P)30 and 6 months.[27,28] This suggests that rod photoreceptor cells function normally, but their density is simply reduced in the KO mouse. The biological origin of this thin ONL in the KO mouse remains unexplained. Is the ONL born thin, or is it normal and then degenerates?

In addition to mediating cone pigment regeneration, IRBP may have other roles. It is possible that IRBP plays a role in eye development.[29,30] IRBP mRNA appears at embryonic day (E)13[31] and the protein is detected at E17.[32] Though this early expression is roughly coincident with cone photoreceptor birth,[33,34] it is well before mouse eyes open. What is the purpose of this precocious expression?

If IRBP plays a role in eye development, the eye of the KO mouse should develop abnormally. To test this hypothesis, we measured the birth and death of retinal cells, the thicknesses of retinal cell layers, the dimensions, weight, and refractive power of KO and WT mouse eyes from early postnatal stages to adulthood. The results revealed a profound myopic shift and an enlarged posterior segment in the KO mouse. Further, our experiments reveal that the retinal thinning in the IRBP KO mouse at P30[27] results from a surge in photoreceptor cell

Investigative Ophthalmology & Visual Science, July 2011, Vol. 52, No. 8

apoptosis that starts at P23 and peaks at P25. We conclude that IRBP has a role in controlling eye growth in development and a subsequent role in maintenance of retinal health.

Methods

Mouse Strains

KO mice[27] used in these experiments (originally created in 129/Ola embryonic stem cells[35]) were backcrossed[36] against C57BL/6J for 10 generations. C57BL/6J mice were used as wild-type (WT) controls. Food and water were provided ad libitum, with 12:12 light-dark cycling. Genotypes were verified with specific primers[24] in all breeds, both KO and WT. The ERG phenotype in the KO was reduced by 40% of the WT a-wave magnitude at P30 as previously shown[27] validating use of the current KO mice in this study. We adhered to the ARVO Statement for the Use of Animals in Ophthalmic and Vision Research. The Emory IACUC approved these studies.

Histology and Morphometrics

We followed the recommendations of Howland and Howland[37] for nomenclature of axes and planes in the mouse eye, as indicated in Figure 1. Histologic and morphometric procedures followed standard techniques.[38,39] Sections were cut on a vertical (sagittal) plane through the optic nerve head (ONH) and the center of the cornea (Fig. 1). Paraffin sections were used for bromodeoxyuridine (BrdU), TUNEL, cone-arrestin staining, and hematoxylin and eosin (H&E) staining. BrdU labeling (BrdU Labeling Reagent, Invitrogen, Carlsbad, CA) and TUNEL staining (DeadEnd Fluorometric TUNEL System, Promega, Madison, WI) followed the manufacturer's instructions. Cone cell counting used an antibody specific to mouse cone arrestin (mCar/LUMIJ).[40,41] Other eyes were embedded in epon 802. Sections were cut at 1-μm thickness and stained with toluidine blue. Plastic sections were used for counting the number of nuclei in nuclear layers, measuring retinal arc length along a vertical great meridian (Fig. 1; retinal arc length, hereafter), and measuring layer thicknesses (Longboard V7.5; ImagingPlanet, Goleta, CA). "ONL nuclei counts" are defined here as the number of nuclei on a perpendicular line crossing the thickness of the ONL. In this study, layer thicknesses and ONL nuclei counts were made at 250-μm steps from the optic nerve head to the far periphery in both inferior and superior halves of the retina. These increasingly eccentric measurements were made until there was no more retina to count. In counting other layers (inner nuclear layer [INL], ganglion cell layer [GCL], etc.) and cones, which had rarer numbers of objects, at each 250-μm step, a 100-μm wide column (also known as box or bin) running along the retinal arc was counted. All these measurements were averaged per section from each eye.

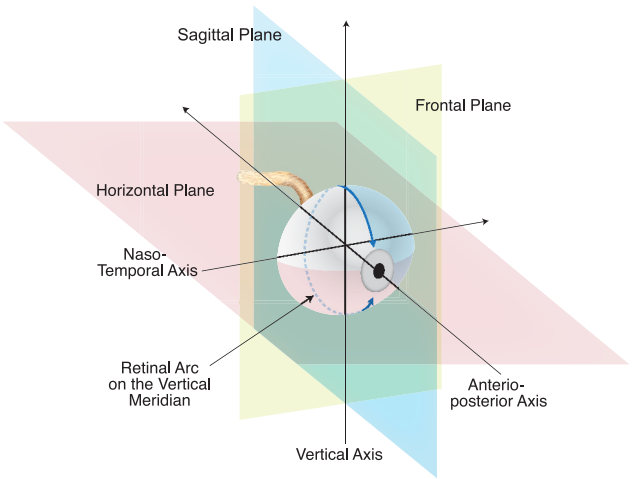

Figure 1. Naming conventions recommended by Howland and Howland[37]for planes and axes of the vertebrate eye regardless of species. A histologic section cut on the vertical plane through the great meridian is illustrated. The *double arrowheads* indicate the "retinal arc length" along the vertical meridian. The horizontal, vertical, and frontal planes are marked, as are the anterior-posterior (A-P) axis (also known as optic axis), the nasal-temporal (N-T) axis, and the superior-inferior (S-I; vertical) axis.

Refractive Power

Unless stated otherwise, readings were taken on both eyes of each mouse and then averaged to generate a single measurement per mouse. Eyes were refracted with an infrared photorefractor modified for mouse eyes.[42–44] Pupils were dilated with 1% (wt/vol) ophthalmic grade tropicamide in both eyes. Measurements were only taken when the pupil was larger than 2.0 mm. Three to six measurements per eye per mouse were recorded. Once the awake measurements were conducted, the mouse was anesthetized with ketamine and xylazine (80 mg and 16 mg per kg body weight) and the refractions were repeated in each eye.[43] Longitudinal assessments of KO and WT were made at P30, P45, and P60.

We assessed axial length by partial coherence interferometry (PCI)[45] and noncontact laser micrometry (LM)[46] at P30, P45, and P60. The PCI was a custom-built system[45] modified for the mouse eye and enabled in vivo measurements of anterior-posterior (A-P) axial length from the surface of the cornea to the RPE/choroidal peak. Ex vivo, laser micrometry was used to measure A-P, superior-inferior (S-I), and nasal-temporal (N-T) external eye dimensions, as previously described.[46]

Statistical Analyses

All data are reported as mean and standard deviation (SD). Error bars in figures represent SD. Comparisons are made between two groups, KO and age-matched WT mice by two-tail, two-sample equal variance Student's *t*-test (Excel; Microsoft, Redmond, WA). The number of mice in each group is presented in the Results section, table, or figure legends. A single asterisk represents significant differences at $P < 0.05$, and double asterisks denote significant differences at $P < 0.01$ throughout.

Results

Photorefraction and Ocular Growth Measures

In a longitudinal study, photorefraction and axial length using partial coherence interferometry (PCI) was measured in the same mice at P30, P45, and P60 (Fig. 2). The eyes grew axially with corresponding changes in refractive power from P30 to P60 in both WT and KO mice. A-P length was significantly greater in the KO mouse at every age (e.g., 3.498 ± 0.0351 mm vs. 3.286 ± 0.0506 mm at P60; Fig. 2), and KO mice were significantly less hyperopic at each age compared with WT mice (e.g., −4.56 ± 0.70 D vs. 9.98 ± 0.993 D at P60; Fig. 2).

A-P, S-I, and N-T external dimensions (Fig. 1) of WT and KO mouse eyes were measured[46] at P60 (Table 1). Each axis was longer in the KO mouse than the WT ($P < 0.05$, in each comparison), as measured by a noncontact laser micrometer.[46] This indicated an enlarged globe in the KO mouse. Eye weights were consistent with eye size: the KO mouse eye was heavier by 28% ($P < 0.05$) than the WT. This was despite the same whole body weight in both groups (Table 1).

Given the severe myopic shift and the enlarged eye of the KO mouse, histologic cross-sections of KO mouse eyes should have a longer retinal arc length (Fig. 1) than WT. A representative histologic image of one half of a cross-sectional retinal arc from a P30 WT mouse is shown in Figure 3, along with a corresponding retinal arc from a P30 KO. From the ONH to the ora serrata, the arc length was 15% longer in KO mice compared with WT, as predicted. Further data corroborated this

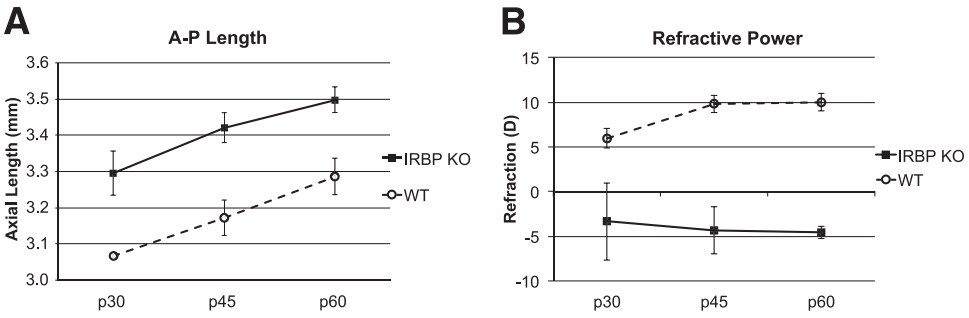

FIGURE 2. (**A**) Partial coherence interferometry and (**B**) photorefractions following mice longitudinally. The same mice were measured at P30 through P60, and another group from P45 to P60. Refractions were measured with a photorefractor. Data are presented as mean ± SD. From P30 to P60, the mouse eyes continue to elongate on the A-P axis. At each age the KO eyes are significantly longer. At the same time, the KO mice became relatively more myopic, and the WT mice became more hyperopic. For KO mice at P30, refractions were performed on three mice and axial length was measured on four mice. For KO mice at P45 and P60, refractions and axial lengths were measured on nine mice. For WT mice at P30, four mice were refracted, and axial lengths were measured on five mice. For WT mice at P45 and P60, refractions and axial lengths were measured on five mice.

observation: the retina arc lengths from numerous litters during development are summarized in Figure 4. Mice from independent litters in each group (KO and WT) were measured at each age. Up to P7, arc lengths did not vary between KO and WT. However, from P10 on, the retina arc length averaged 18% larger in the KO compared with age-matched WT (Fig. 4). In the mouse, there is no space between the outermost tip of the retina and the ciliary body in either the WT or the KO. Any variation in size of the retina is reflected in a concomitant variation in size of the entire posterior segment. The KO retina and posterior segment are enlarged relative to WT. Retina arc length measurements in paraffin sections (data not shown) confirmed all the measurements in plastic sections.

Retinal Morphology Changes During Development

Retinal morphology was examined during development in KO and WT mice. At P10 and younger, the INL and ONL are not resolved and the elongated nuclear shape makes it difficult to count individual nuclei. However, it was possible to measure the thickness of retina layers (Fig. 5). The results showed little difference in the average thickness of the ONL of KO and age-matched WT from P2 to P10. At P12, the average ONL thickness of WT mice ($n = 3$) was 54.0 ± 3.29 μm while that of KO mice ($n = 4$) was 44.1 ± 2.44 μm ($P < 0.01$), an 18.3% difference. These data show that the initiation of retinal thinning in the ONL of the KO mouse started between P10 and P12. However, as described later, this thinning was not accompanied by apoptotic loss of nuclei.

At stages later than P10, nuclei were counted across the ONL of KO and WT mouse retinas. At P12 and P15, WT and KO mice had a comparable number of nuclei (Fig. 6). At P18, the number of nuclei per ONL was lower in KO by 23% compared with WT ($P < 0.05$; $n = 3$ mice for both strains), with similar differences persisting at P20 and P25 (Fig. 6).

Between P25 and P30, the number of nuclei per ONL decreased further (38% decrease) in the KO compared with WT (Fig. 6). From P30 through P440 there was a gradual decrease in the ONL nuclear count in KO mice, which resulted in an ONL only three nuclei thick (Fig. 7) while the WT remained stable at 8 to 9 nuclei throughout the study period. This decrease at older ages is likely due to apoptotic photoreceptor cell death reflecting retinal degeneration as discussed later.

Rod inner segments (RIS) of the KO mice were 28% shorter compared with WT (13.6 ± 1.4 μm KO and 18.9 ± 0.76 μm for WT; $P < 0.01$; $n = 3$ in WT and $n = 4$ in KO mice). KO rod outer segments (ROS) at P30 were more disorganized. Also, there was irregular spacing not observed in WT between the normally well-ordered nuclear columns (also known as stacks or cords of nuclei[47]) in the ONL of the KO retina (Fig. 3).

To determine whether the percentage loss of cones was the same as that of rods in the KO, immunoreactive cone arrestin-positive cells were counted in the retina. Paraffin sections were immunostained with an antibody against cone arrestin (LUMIJ), which was used because it exhibits broad cone photoreceptor-specificity.[41,48] The cone density averaged 30% less in the KO than WT ($P < 0.001$, $n = 6$ mice in both KO and WT, P30, Fig. 8; same results at P330, data not shown). This decrease in cones is similar to the loss of ONL shown in Figure 6.

The density of nuclei in the INL was measured at increasing eccentricities across the retina arc (Fig. 9) in WT and KO (both $n = 3$) at P30 in the superior and inferior halves of the retina. The KO INL was always thinner than the WT, except at the farthest periphery near the ora serrata, where they were the same. In superior retina, the INL averaged 67.5 ± 6.55 nuclei per 100-μm bin in WT and KO averaged 52.5 ± 2.33 (23.8% lesser density in the KO; $P < 0.01$). In the inferior retina, WT had 68.9 ± 4.55 and KO had 55.0 ± 3.64 nuclei per bin (KO had 18.6% reduced density; $P < 0.05$). The thinning of the INL is similar in magnitude to early stage (P10–P25) thinning of the ONL in the KO retina (Fig. 6), but the INL did not degenerate further as the ONL did after P25.

Cell Birth and Death

The preceding data support the hypothesis that up to P25, reduced INL and ONL cell density in KO mice is due to spreading of the retina over a larger surface area. Two other

TABLE 1. P60 Laser Micrometer External Axes Data, Mouse Whole Body, and Eye Weight

Strain	*N*	Whole Body Weight (g)	Eye Weight (mg)	Axial (mm)	Nasal-Temporal (mm)	Superior-Inferior (mm)
WT	18	19.7 ± 3.8	16.3 ± 1.6	3.231 ± 0.069	3.185 ± 0.079	3.162 ± 0.092
KO	13	20.1 ± 2.0	21.3 ± 0.8	3.532 ± 0.042	3.425 ± 0.069	3.400 ± 0.071

The IRBP KO mouse eyes are heavier, larger, and longer axially by external measures, $P < 0.01$, compared with WT. Mouse body weights at P60 are all the same between WT and KOs. Data are presented as mean ± SD.

FIGURE 3. Early lengthening and thinning of the IRBP KO mouse retina. Retina arc length and morphology at P30. (**A**) IRBP knockout (KO). (**B**) C57BL/6J (WT). The neural retina of the KO mouse at P30 directly abuts the ciliary body. There was no differential thinning of the retina at the tip abutting the pars plana. The arc length of the neural retina between the ONL and inner plexiform layer (IPL) was measured on the superior half of the eye. The WT arc length was 2397 μm, and the KO arc length was 2752 μm, or 15% longer. This increased arc length in the KO mouse is representative of the data. The KO retina exhibited a 40% thinning of the ONL and evidence of rod outer segment (ROS) disorganization. ROS, rod inner segment (RIS), and INL exhibited approximately 20% thinning. Scale bar, 250 μm.

independent hypotheses might account for this reduced cell density. First, fewer cells might be born in the ventricular zone, leading to thinner layers in the KO. Second, increased cell death would reduce layer thickness. We used BrdU birth dating to test the first possibility and TUNEL staining to test the second.

As shown in Figure 10, BrdU labeling and immunostaining demonstrated that there was little difference in the number of dividing cells between the KO and WT retinas from P2 to P10. At early stages (P2 and P4), there were numerous dividing cells in the ventricular zone of the retina, but at matched ages there was no difference between the KO and WT mouse. At P7 and P10 there were few dividing cells but again no difference between WT and KO.

To test whether apoptotic cell death accounted for an eventual difference in the number of photoreceptor cells between KO and WT, TUNEL-positive cells in sections from P2 to P30 retina were counted. As shown in Figure 11A, there were no significant differences in the numbers of TUNEL-positive cells between KO and WT at P2 and P4. Unexpectedly, at P7 and P10 there was a trend toward more apoptosis in the INL of the WT, and a significant increase in TUNEL-positive cells in the WT mouse over the KO at P12 as well (Fig. 11A). This timing coincides with the extension of retinal arc length in the KO. As shown in Figure 11B, in the ONL from P15 through P22 there was a low level of apoptosis and no difference between KO and WT. Conversely, starting at P23 to P30 there were far more apoptotic cells in KO ONL. In the KO at P25, there were five times as many apoptotic nuclei (15.1 $\pm$ 2.46 cells per retina, $n = 5$; than WT (2.81 $\pm$ 1.75; $n = 5$) ($P < 0.00001$).

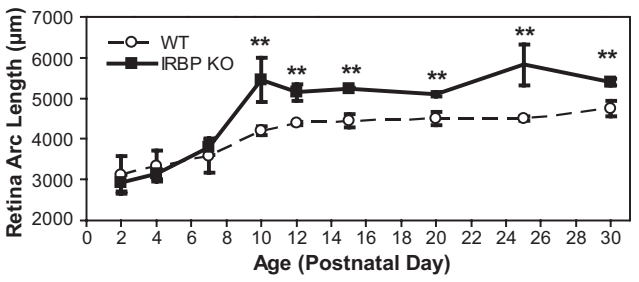

FIGURE 4. Retina arc length in developing mice. The arc length of the neural retina was measured from one pars plana to the other through the ONH on the vertical meridian. The arc length was measured at the interface of the ONL and the inner plexiform layer (IPL). Measurements were made at the indicated postnatal ages ranging from P2 to P30. The results showed a substantially longer arc length in the KO mouse starting at P10, suggesting that the posterior segment of the KO mouse eye is larger than the WT eye. The number of mice per group varied, but was always three or more. At P2, $n = 3$, both KO and WT. At P4, $n = 3$ WT, and $n = 4$ KO. At P7, $n = 4$ both WT and KO. At P10, $n = 4$ both WT and KO. At P12, $n = 3$ WT, and $n = 4$ KO. At P15, $n = 3$ WT, and $n = 4$ KO. At P20, $n = 5$ WT, and $n = 4$ KO. At P25, $n = 4$ WT, and $n = 3$ KO. At P30, $n = 3$ for both WT and KO. $^{**}P < 0.01$.

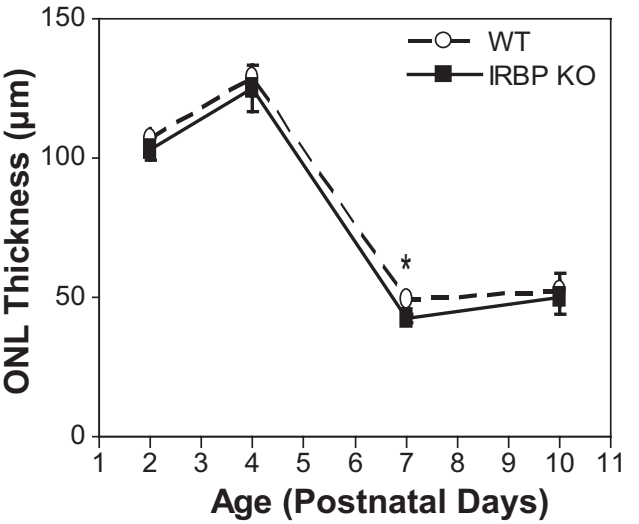

FIGURE 5. Very early postnatal ONL thicknesses are normal in IRBP KO mouse. Thickness measurements were made at increasing eccentricities of 250-μm increments from the ONH to the edges of the retina. These were averaged across the retina surface. The number of mice per group varied, but was always 3 or more. For all WT groups the sample size was three mice per group. For the KO groups, the sample size was four mice per group except P7, which had a sample size of three mice. Error bars represent standard deviations. ONL thicknesses were almost identical comparing WT to KO from P2 through P10.

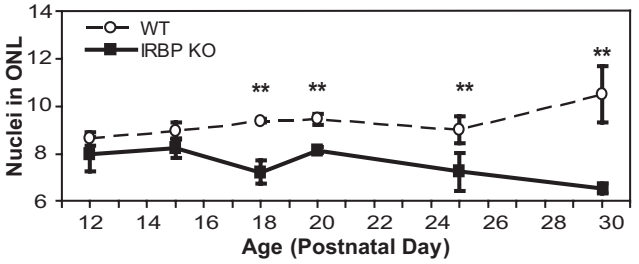

FIGURE 6. Counts of the ONL during development. Nuclei in the ONL were counted along sections cut on a vertical meridian at intervals of 250 μm across the retina in superior and inferior halves in WT and KO mice. These were averaged across the retina surface. Three mice from independent litters were measured at each age in each group (KO and WT). From P18 on, there were fewer nuclei across the ONL of the KO than in the WT mouse. $^{**}P < 0.01$.

In summary, there was more apoptosis at P7–P12 in the WT in the INL. This reflects normal pruning[49] in theWT mouse eye and appears to not occur in the KO. About two weeks later, there was a burst of apoptosis peaking at P25 in the ONL of the KO, coinciding with substantial degeneration of the ONL in the KO.

DISCUSSION

Our data suggest that IRBP is required in development for proper eye growth and required subsequently for retinal health. The absence of IRBP results in an extraordinary myopic shift and a temporally distinct apoptotic degeneration of the ONL. The IRBP KO mouse develops a large myopic shift that is consistent with developmental abnormalities in eye size and shape (Fig. 2, Table 1). There is a simultaneous axial elongation. Elongation may not be the sole cause of the differences in refraction, but we noted no differences in lens thickness or diameter or weight comparing KO to WT (data not shown). We did not measure surface curvatures or anterior chamber depth. The origin of excess axial length that contributed to the

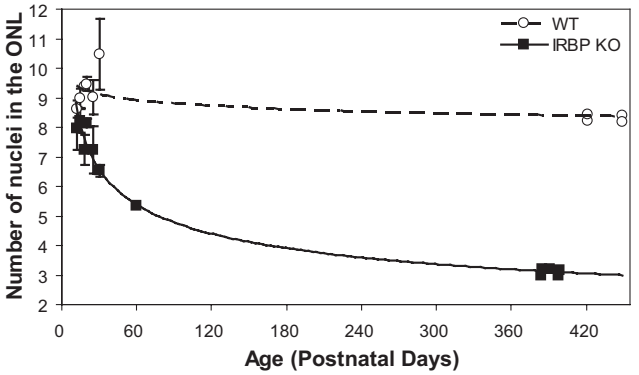

FIGURE 7. Retinal degeneration during aging of the IRBP KO mouse. ONL counts in cords across the retina is illustrated[62,63] in aging KO and WT mice. ONL nuclei counts at 250-μm intervals were averaged and plotted according to the postnatal age of the mouse. From P60 on, each point represents a single mouse. Before P60, each group contained three mice, except P25, which had four mice each. Plastic sections were used. The IRBP KO mouse lost about two-thirds of ONL thickness in a year, typical of a slow retinal degeneration. In KO mice that died due to old age, in excess of two years old, the ONL was one nucleus or less in ONL thickness (data not shown). The WT ONL thickness remained almost unchanged at 8 to 9 nuclei thick in one- to two-year-old mice. The loss of nuclei in the KO retina is significant in mice older than 1 year of age ($P < 0.01$; $n = 4$ WT, $n = 5$ KO).

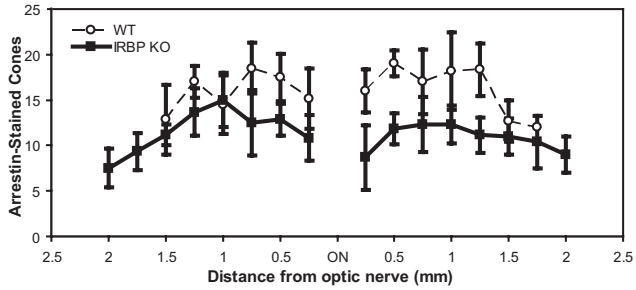

FIGURE 8. Cone-arrestin staining in the P30 retina. Cone-arrestin positive cells were counted at intervals across the retina, along the vertical meridian. Cone arrestin was immunostained (LUMIJ antibodies), and positive cells counted within bins of 100 μm every 250 μm, measured from the ONH. Because the KO retinas were longer in arc length, two more bins were counted superiorly at the pars plana, and one extra bin was counted on the inferior. There were more cone-arrestin positive cells in the WT than KO, with approximately 24.8% ($P < 0.001$) and 34.5% ($P < 0.0001$) more cones in the inferior and superior portions of the WT compared with the KO. One eye was analyzed from one animal, in each of 6 litters, in KO and in WT, at P30.

myopic shift is observed early in development. Comparing WT and KO, the critical change in eye growth occurred in a distinct and short time period in early postnatal development. Until P7, eye growth was the same in the WT and KO. After P7 and before P10, the KO mouse eye enlarged significantly more than in the WT (Figs, 4, 6, and 10). This time period is coincident with insufficient pruning of the INL in the KO mouse (Fig. 11) but is well before photoreceptor degeneration in the KO strain, which we now show here to begin shortly after weaning at P23 and to peak at P25 (Fig. 11B).

The IRBP KO mouse may help us to learn of relationships between prevision and later vision-dependent eye development. There is great interest in how vision-dependent adaptive processes and vision-independent genetically-determined eye growth might interact.[50] If or how these two processes interact are open questions. It remains unclear how the myopic shifts (measured at P30–P60) and globe enlargement (starting at P10) in the IRBP KO mouse are caused. But because IRBP deficits affect both emmetropia and early eye size, it is possible that further study of IRBP might reflect on putative interactions of vision-dependent and vision-independent eye growth.[50] Future work is needed to test biochemical pathways affected by the absence of IRBP.

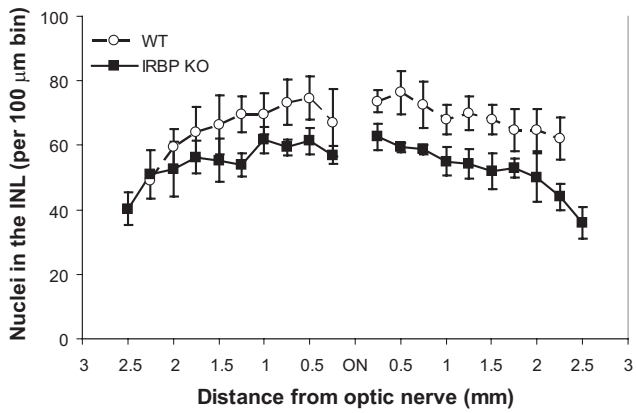

FIGURE 9. The inner nuclear layer (INL) is thinner in the IRBP KO mouse at P30. Nuclei counts in the INL were conducted at 250-μm intervals from the ONH, and bins of 100 μm were counted and averaged. One eye was analyzed from one animal, in each of 3 KO litters and 5 WT litters. Error bars represent the standard deviations.

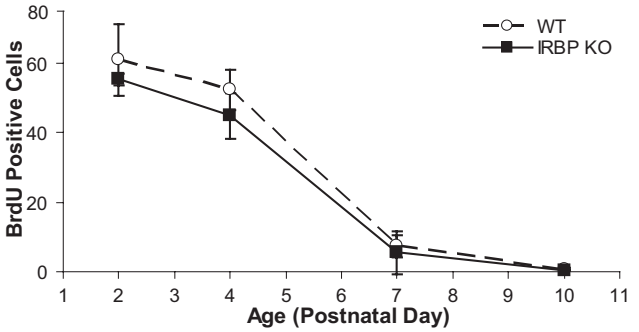

FIGURE 10. Cell birth in the IRBP KO and the WT mouse are the same from P2 to P10. Bromodeoxyuridine (BrdU) was used to label cells actively undergoing scheduled DNA synthesis. BrdU-positive cells in the ventricular zone of the retina were counted in sections cut on the vertical meridian. Bins of 100 μm were counted every 250 μm, and averaged across the whole retina. One eye was analyzed from one animal, in each of 4 litters at each age, except at P4: three for WT, and at P10, three for KO. No significant difference was detected between WT and KO at any age. Images indicated active scheduled DNA synthesis and cell division at P2 and P4 in both WT and KO mouse retinas; however, there was no difference in the number of labeled nuclei between WT and KO mice. There was approximately 10% as much labeling at P7 than at either P2 or P4, and almost no labeling at P10 suggesting that cell division in the ventricular zone was complete by P10.

It is hypothetically possible that signaling molecules are shared between the two processes for vision-dependent and vision-independent eye growth. For example, it is possible that local intraocular "growth control affectors" (the neurotransmitter dopamine and the morphogen retinoic acid [RA] are exemplars) that originate within the local retina must pass through the interphotoreceptor space (IPS; also known as the subretinal space) to reach the RPE and to send information to choroidal and scleral targets.[51] Within the IPS, IRBP constitutes the majority of soluble protein. Whether physiologically relevant or not, growth control signals from the retina must interact with or avoid IRBP if they transit the IPS. For instance, IRBP binds RA at high affinity,[2,52–55] which is known to regulate eye growth[56] and inhibit scleral proteoglycan synthesis.[57] Thus, IRBP may act as a gatekeeper for RA in eye growth.

Another possibility is that IRBP may act by regulating cell fate in the inner retina. We found that the INL of the developing IRBP KO mouse retina undergoes reduced stage-specific apoptosis, suggesting that absence of IRBP prevents correct developmental pruning. Lack of IRBP could lead to an aberrant retinal cell population (with a cell body in the INL) that sends improper signals to growth targets. For instance, IRBP could affect the development of GABAergic amacrine or ON-bipolar cells[58] and affect intracellular transduction of regulatory stimuli.

Spreading and thinning of the retina in young IRBP KO pups were demonstrated by histologic and morphometric approaches. The KO retina elongated on a vertical arc by approximately 20% in a burst between P7 and P10 (Fig. 4). Thereafter, the KO retina maintains a 20% longer arc length, as the mouse eye grows. The KO ONL was thinner by mensuration at P12, and at P18, the KO ONL had noticeably fewer nuclei (Fig. 6), both accounted for by spreading, with no evidence of apoptosis in the KO ONL at these ages (P7–P18). Though artifactual histologic and selective shrinkage of the KO retina is possible, the ONL counts (which are not subject to the same potential problem as thickness measurements) support actual thinning. Also, in tree shrew the retina thins and spreads to cover the enlarged globe in form deprivation myopia, and histologic retinal layer thicknesses are the same as in the living retina measured by spectral domain optical coherence tomography.[59]

A critical period in KO and WT eye development occurred at P23 to P25, when the ONL in the KO abruptly began to experience high levels of apoptotic cell death. TUNEL counts indicate that apoptotic cell death is the dominant process controlling the decrease in ONL thickness at P23 to P30 in the KO (Fig. 11B). After P30, a gradual but substantial loss of the ONL occurs over the remaining lifespan of the mouse. This burst of apoptosis at P23 to P25 explains the previously unknown temporal origins and mechanism of photoreceptor cell death in the retinal degeneration in the IRBP KO mouse.

At one month of age and older, one prior study showed a substantially thinner ONL in the KO mouse.[27] This phenotype has remained unchanged over the 10-plus years (and approxi-

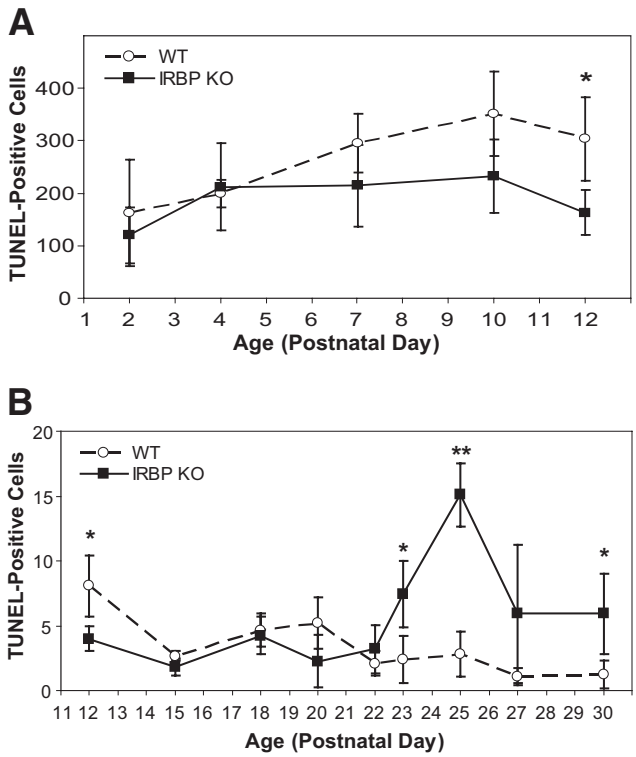

FIGURE 11. (**A**) Normal pruning in the INL of the IRBP KO mouse is diminished at P7 to P12. Programmed cell death in the WT and KO mouse retina was measured. TUNEL-positive cells were counted in the whole retina at the indicated postnatal ages. No significant differences were detected at P2 and P4. There was a trend of more TUNEL-positive cells at P7 and P10 in the WT, but the differences were not significant. There were more TUNEL-positive cells in WT at P12 than in the KO mouse ($P < 0.05$). One eye was analyzed from each animal. Per group, the sample size was four mice at P2, P10, and P12. At P4 and P7, the sample size was five mice per group. The errors bars designate SD. A single asterisk denotes a significant difference at $P < 0.05$. At P7 and P10, TUNEL-positive nuclei were located in the developing INL, in both WT and KO retinas, suggestive of normal pruning in the INL in WT. This normal pruning was reduced in the KO mouse. (**B**) Summary of TUNEL-positive cell counts in the ONL of P12 to P30 mice. There was a burst of apoptosis in the KO mouse retinas starting at P23 and continuing through P30. The peak was at P25, with roughly five times as many TUNEL-positive cells in the KO mouse than the WT mouse ONL. The difference was significant at $P < 0.00001$. Afterward, there continued to be more apoptotic cell death in the KO than the WT mouse ONL. $n = 4$ mice from independent litters at P12–P18 for both WT and KO. At P20, $n = 3$ for WT, and $n = 4$ for KO. At P22 and P23, $n = 4$ for WT and $n = 5$ for KO. At P25, $n = 5$ for both WT and KO. At P27, $n = 4$ for WT and $n = 5$ for KO. At P30, $n = 6$ for both WT and KO. $^{*}P < 0.05$, $^{**}P < 0.01$.

mately 30 generations of breeding) since this mouse was first described. We observed a 38% reduction in ONL counts ($P < 0.01$) at P30 (Fig. 6). Also, the INL, RIS, and ROS were thinner in the KO compared with WT, and the ROS were more sparse and disorganized (Figs. 3 and 9). The retinal degeneration continued to progress by slow loss of the ONL (Fig. 7) as is characteristic of many retinal degenerations and forms of RP.

Cones account for approximately 3% of the photoreceptors in the WT mouse.[60,61] Cone counts in Figure 8 indicate a 30% decrease in cone density in vertical cross-sections of the KO mouse at P30, which is slightly less loss than in the ONL at the same age. Parker et al.[23] find that cone cell densities in flat mounts of isolated retinas are the same in KO and C57BL/6 from one to nine months of age. This seems inconsistent with the present measurements of cone densities on a vertical meridian. It may be accounted for by known differences in preparation, fixation, and by use of antibodies against different cone-specific antigens. Also, the C57BL/6 mice at two different institutions (Emory versus Medical University of South Carolina) appear to originate from two different sources (c.f., Jackson C57BL/6J versus Harlan C57BL/6) with potential genetic drift. These differences remain to be resolved.

Many retinal cells pass through S-phase[33,34] at P2 and P4, and progressively fewer at P7 and P10. There was no difference in BrdU-labeled cell counts between age-matched KO and WT (Fig. 10), suggesting that differential cell division rates did not account for the reduced ONL thickness in the KO mouse. This suggests that the critical difference is the reduced amount of apoptotic pruning of the INL cells at P7 to P10 caused by the deficiency of IRBP in the KO (Fig. 10). Likely, this early apoptosis in WT represents normal retina remodeling in the INL that fails when IRBP is absent. This failure is associated with the large myopic shift and the increased globe size in the KO mouse.

Conclusions and Future Directions

We ruled out the possibility that the ONL was simply born thin in the KO mouse: the ONL is born normal in thickness. Our data revealed two distinct disease processes in the IRBP KO mouse eye. First, starting between P7 and P10, a lengthening of the posterior segment concomitant with insufficient INL pruning results in substantial enlargement of the eye developmentally. This occurs before the eyelids open, suggesting a light-independent mechanism. Second, much later (P23–P25), sudden apoptotic cell death, peaking at P25, in the ONL of the KO mouse results in retinal degeneration, which continues to progress as the KO mouse ages. The temporal separation between the early aberrant posterior segment growth and later photoreceptor degeneration raises the possibility that these two disease processes are largely independent of each other, or require two different functions of IRBP. Alternatively, the later retinal degeneration may be a direct consequence of globe elongation. To test these hypotheses, conditional knockouts of IRBP, knockdowns, and other experiments are needed. These future studies will advance our understanding of the types and etiology of human eye disease caused by IRBP mutations.

Finally, knowledge of how a deficiency in IRBP causes the myopic shift would help in understanding the mechanisms and steps involved in normal eye growth. It is possible that IRBP is an essential intraocular gatekeeper in mechanisms controlling eye growth and emmetropia.

References

1. Gonzalez-Fernandez F, Baer CA, Ghosh D. Module structure of interphotoreceptor retinoid-binding protein (IRBP) may provide bases for its complex role in the visual cycle - structure/function study of Xenopus IRBP. *BMC Biochem.* 2007;8:15.
2. Nickerson JM, Li GR, Lin ZY, Takizawa N, Si JS, Gross EA. Structure-function relationships in the four repeats of human interphotoreceptor retinoid-binding protein (IRBP). *Mol Vis.* 1998;4:33.
3. Lin ZY, Si JS, Nickerson JM. Biochemical and biophysical properties of recombinant human interphotoreceptor retinoid binding protein. *Invest Ophthalmol Vis Sci.* 1994;35:3599–3612.
4. Lin ZY, Li GR, Takizawa N, et al. Structure-function relationships in interphotoreceptor retinoid-binding protein (IRBP). *Mol Vis.* 1997; 3:17.
5. Gross EA, Li GR, Ruuska SE, Boatright JH, Mian IS, Nickerson JM. Effects of dispersed point substitutions in Repeat 1 of human interphotoreceptor retinoid binding protein (IRBP). *Mol Vis.* 2000; 6:40–50.
6. Gross EA, Li GR, Ruuska SE, Boatright JH, Nickerson JM. G239T mutation in Repeat 1 of human IRBP: possible implications for more than one binding site in a single repeat. *Mol Vis.* 2000;6: 51–62.
7. Pfeffer B, Wiggert B, Lee L, Zonnenberg B, Newsome D, Chader G. The presence of a soluble interphotoreceptor retinol-binding protein (IRBP) in the retinal interphotoreceptor space. *J Cell Physiol.* 1983;117:333–341.
8. van Veen T, Katial A, Shinohara T, et al. Retinal photoreceptor neurons and pinealocytes accumulate mRNA for interphotoreceptor retinoid-binding protein (IRBP). *FEBS Lett.* 1986;208:133–137.
9. Porrello K, Bhat SP, Bok D. Detection of interphotoreceptor retinoid binding protein (IRBP) mRNA in human and cone-dominant squirrel retinas by in situ hybridization. *J Histochem Cytochem.* 1991;39:171–176.
10. den Hollander A, McGee TL, Ziviello C, et al. A homozygous missense mutation in the IRBP gene (RBP3) associated with autosomal recessive retinitis pigmentosa. *Invest Ophthalmol Vis Sci.* 2009;50:1864–1872.
11. Abe T, Wiggert B, Bergsma DR, Chader GJ. Vitamin A receptors. I. Comparison of retinol binding to serum retinol-binding protein and to tissue receptors in chick retina and pigment epithelium. *Biochim Biophys Acta.* 1977;498:355–365.
12. Adler AJ, Evans CD, Stafford WF. Molecular properties of bovine interphotoreceptor retinol-binding protein. *J Biol Chem.* 1985; 260:4850–4855.
13. Chen Y, Saari JC, Noy N. Interactions of all-trans-retinol and long-chain fatty acids with interphotoreceptor retinoid-binding protein. *Biochemistry.* 1993;32:11311–11318.
14. Adler AJ, Spencer SA. Effect of light on endogenous ligands carried by interphotoreceptor retinoid-binding protein. *Exp Eye Res.* 1991;53:337–346.
15. Carlson A, Bok D. Promotion of the release of 11-cis-retinal from cultured retinal pigment epithelium by interphotoreceptor retinoid-binding protein. *Biochemistry.* 1992;31:9056–9062.
16. Okajima TI, Pepperberg DR, Ripps H, Wiggert B, Chader GJ. Interphotoreceptor retinoid-binding protein: role in delivery of retinol to the pigment epithelium. *Exp Eye Res.* 1989;49:629–644.
17. Edwards RB, Adler AJ. IRBP enhances removal of 11-cis-retinaldehyde from isolated RPE membranes. *Exp Eye Res.* 2000;70:235–245.
18. Wu Q, Blakeley LR, Cornwall MC, Crouch RK, Wiggert BN, Koutalos Y. Interphotoreceptor retinoid-binding protein is the physiologically relevant carrier that removes retinol from rod photoreceptor outer segments. *Biochemistry.* 2007;46:8669–8679.
19. Tsina E, Chen C, Koutalos Y, et al. Physiological and microfluorometric studies of reduction and clearance of retinal in bleached rod photoreceptors. *J Gen Physiol.* 2004;124:429–443.
20. Qtaishat NM, Wiggert B, Pepperberg DR. Interphotoreceptor retinoid-binding protein (IRBP) promotes the release of all-trans retinol from the isolated retina following rhodopsin bleaching illumination. *Exp Eye Res.* 2005;81:455–463.
21. Ho MT, Pownall HJ, Hollyfield JG. Spontaneous transfer of retinoic acid, retinyl acetate, and retinyl palmitate between single unilamellar vesicles. *J Biol Chem.* 1989;264:17759–17763.
22. Lamb TD, Pugh EN. Phototransduction, dark adaptation, and rhodopsin regeneration the proctor lecture. *Invest Ophthalmol Vis Sci.* 2006;47:5138–5152.

23. Parker RO, Fan J, Nickerson JM, Liou GI, Crouch RK. Normal cone function requires the interphotoreceptor retinoid binding protein. *J Neurosci.* 2009;29:4616–4621.
24. Palczewski K, Van Hooser JP, Garwin GG, Chen J, Liou GI, Saari JC. Kinetics of visual pigment regeneration in excised mouse eyes and in mice with a targeted disruption of the gene encoding interphotoreceptor retinoid-binding protein or arrestin. *Biochemistry.* 1999;38:12012–12019.
25. Wang JS, Estevez ME, Cornwall MC, Kefalov VJ. Intra-retinal visual cycle required for rapid and complete cone dark adaptation. *Nat Neurosci.* 2009;12:295–302.
26. Jin M, Li S, Nusinowitz S, et al. The role of interphotoreceptor retinoid-binding protein on the translocation of visual retinoids and function of cone photoreceptors. *J Neurosci.* 2009;29:1486–1495.
27. Liou GI, Fei Y, Peachey NS, et al. Early onset photoreceptor abnormalities induced by targeted disruption of the interphotoreceptor retinoid-binding protein gene. *J Neurosci.* 1998;18:4511–4520.
28. Ripps H, Peachey NS, Xu X, Nozell SE, Smith SB, Liou GI. The rhodopsin cycle is preserved in IRBP "knockout" mice despite abnormalities in retinal structure and function. *Vis Neurosci.* 2000;17:97–105.
29. Gonzalez-Fernandez F, Healy JI. Early expression of the gene for interphotoreceptor retinol-binding protein during photoreceptor differentiation suggests a critical role for the interphotoreceptor matrix in retinal development. *J Cell Biol.* 1990;111:2775–2784.
30. Gonzalez-Fernandez F. Interphotoreceptor retinoid-binding protein–an old gene for new eyes. *Vision Res.* 2003;43:3021–3036.
31. Liou GI, Wang M, Matragoon S. Timing of interphotoreceptor retinoid-binding protein (IRBP) gene expression and hypomethylation in developing mouse retina. *Dev Biol.* 1994;161:345–356.
32. Carter-Dawson L, Alvarez RA, Fong SL, Liou GI, Sperling HG, Bridges CD. Rhodopsin, 11-cis vitamin A, and interstitial retinol-binding protein (IRBP) during retinal development in normal and rd mutant mice. *Dev Biol.* 1986;116:431–438.
33. Young RW. The ninth Frederick H. Verhoeff lecture. The life history of retinal cells. *Trans Am Ophthalmol Soc.* 1983;81:193–228.
34. Rapaport DH, Wong LL, Wood ED, Yasumura D, LaVail MM. Timing and topography of cell genesis in the rat retina. *J Comp Neurol.* 2004;474:304–324.
35. Komano H, Fujiura Y, Kawaguchi M, et al. Homeostatic regulation of intestinal epithelia by intraepithelial gamma delta T cells. *Proc Natl Acad Sci U S A.* 1995;92:6147–6151.
36. Avichezer D, Liou GI, Chan CC, et al. Interphotoreceptor retinoid-binding protein (IRBP)-deficient C57BL/6 mice have enhanced immunological and immunopathogenic responses to IRBP and an altered recognition of IRBP epitopes. *J Autoimmun.* 2003;21:185–194.
37. Howland HC, Howland M. A standard nomenclature for the axes and planes of vertebrate eyes. *Vision Res.* 2008;48:1926–1927.
38. Phillips MJ, Walker TA, Choi H-Y, et al. Tauroursodeoxycholic acid preservation of photoreceptor structure and function in the rd10 mouse through postnatal day 30. *Invest Ophthalmol Vis Sci.* 2008;49:2148–2155.
39. Boatright JH, Moring AG, McElroy C, et al. Tool from ancient pharmacopoeia prevents vision loss. *Mol Vis.* 2006;12:1706–1714.
40. Zhu X, Li A, Brown B, Weiss ER, Osawa S, Craft CM. Mouse cone arrestin expression pattern: light induced translocation in cone photoreceptors. *Mol Vis.* 2002;8:462–471.
41. Zhu X, Brown B, Li A, Mears AJ, Swaroop A, Craft CM. GRK1-dependent phosphorylation of S and M opsins and their binding to cone arrestin during cone phototransduction in the mouse retina. *J Neurosci.* 2003;23:6152–6160.
42. Schmucker C, Schaeffel F. A paraxial schematic eye model for the growing C57BL/6 mouse. *Vision Res.* 2004;44:1857–1867.
43. Pardue MT, Faulkner AE, Fernandes A, et al. High susceptibility to experimental myopia in a mouse model with a retinal on pathway defect. *Invest Ophthalmol Vis Sci.* 2008;49:706–712.
44. Schaeffel F, Burkhardt E, Howland HC, Williams RW. Measurement of refractive state and deprivation myopia in two strains of mice. *Optom Vis Sci.* 2004;81:99–110.
45. Schmid GF, Papastergiou GI, Nickla DL, et al. Validation of laser Doppler interferometric measurements in vivo of axial eye length and thickness of fundus layers in chicks. *Curr Eye Res.* 1996;15:691–696.
46. Wisard J, Chrenek MA, Wright C, et al. Non-contact measurement of linear external dimensions of the mouse eye. *J Neurosci Methods.* 2010;187:156–166.
47. Solovei I, Kreysing M, Lanctôt C, et al. Nuclear architecture of rod photoreceptor cells adapts to vision in mammalian evolution. *Cell.* 2009;137:356–368.
48. Zhang J, Gray J, Wu L, et al. Rb regulates proliferation and rod photoreceptor development in the mouse retina. *Nat Genet.* 2004;36:351–360.
49. Young RW. Cell death during differentiation of the retina in the mouse. *J Comp Neurol.* 1984;229:362–373.
50. Siegwart JT, Norton TT. Perspective: how might emmetropization and genetic factors produce myopia in normal eyes? *Optom Vis Sci.* 2011;88:E365–E372.
51. Rymer J, Wildsoet CF. The role of the retinal pigment epithelium in eye growth regulation and myopia: a review. *Vis Neurosci.* 2005;22:251–261.
52. Rengarajan K, Pohl J, Nickerson J. Photoaffinity labeling of human IRBP with all-trans-retinoic acid. *Biochem Biophys Res Commun.* 2001;284:268–274.
53. Fong SL, Liou GI, Landers RA, Alvarez RA, Bridges CD. Purification and characterization of a retinol-binding glycoprotein synthesized and secreted by bovine neural retina. *J Biol Chem.* 1984;259:6534–6542.
54. Liou GI, Bridges CD, Fong SL, Alvarez RA, Gonzalez-Fernandez F. Vitamin A transport between retina and pigment epithelium–an interstitial protein carrying endogenous retinol (interstitial retinol-binding protein). *Vision Res.* 1982;22:1457–1467.
55. Shaw NS, Noy N. Interphotoreceptor retinoid-binding protein contains three retinoid binding sites. *Exp Eye Res.* 2001;72:183–190.
56. McFadden SA, Howlett MH, Mertz JR, Wallman J. Acute effects of dietary retinoic acid on ocular components in the growing chick. *Exp Eye Res.* 2006;83:949–961.
57. Mertz JR, Wallman J. Choroidal retinoic acid synthesis: a possible mediator between refractive error and compensatory eye growth. *Exp Eye Res.* 2000;70:519–527.
58. Zhong X, Ge J, Smith EL, Stell WK. Image defocus modulates activity of bipolar and amacrine cells in macaque retina. *Invest Ophthalmol Vis Sci.* 2004;45:2065–2074.
59. Abbott CJ, Grünert U, Pianta MJ, McBrien NA. Retinal thinning in tree shrews with induced high myopia: Optical coherence tomography and histological assessment. *Vision Res.* 2011;51:376–385.
60. Jeon CJ, Strettoi E, Masland RH. The major cell populations of the mouse retina. *J Neurosci.* 1998;18:8936–8946.
61. Carter-Dawson LD, LaVail MM. Rods and cones in the mouse retina. I. Structural analysis using light and electron microscopy. *J Comp Neurol.* 1979;188:245–262.
62. Lee ES, Flannery JG. Transport of truncated rhodopsin and its effects on rod function and degeneration. *Invest Ophthalmol Vis Sci.* 2007;48:2868–2876.
63. Boudard DL, Tanimoto N, Huber G, Beck SC, Seeliger MW, Hicks D. Cone loss is delayed relative to rod loss during induced retinal degeneration in the diurnal cone-rich rodent Arvicanthis ansorgei. *Neuroscience.* 2010;169:1815–1830.